Internal conversion in the S_1 $^1B_{3u}$ state of pyrene

Yasuyuki Kowaka[a], Naofumi Nakayama[b], Takayoshi Ishimoto[c], Umpei Nagashima[d,e], Takaya Yamanaka[f], Norifumi Ozawa[a], Masaaki Baba[*,a]

[a]*Division of Chemistry, Graduate School of Science, Kyoto University, Sakyo-ku, Kyoto 606-8502, Japan*
[b]*Conflex Corporation, 2-15-19 Kami-osaki, Shinagawa-ku, Tokyo 141-0021, Japan*
[c]*INAMORI Frontier Research Center, Kyushu University, Motooka 744, Nishi-ku, Fukuoka 819-0395, Japan*
[d]*Research Institute for Nanosystem, National Institute of Advanced Industrial Science and Technology, Umezono 1-1-1, Tsukuba, Ibaraki 305-8561, Japan*
[e]*Core Research for Evolutional Science and Technology, Japan Science and Technology Agency, 4-1-8 Honcho, Kawaguchi 332-0012, Japan*
[f]*Instrument Center, Institute for Molecular Science, Myodaiji, Okazaki 444-8585, Japan*

Abstract

Fluorescence excitation spectra and fluorescence lifetimes at single vibronic levels in the S_1 state have been observed for jet-cooled pyrene. The fluorescence lifetimes at the zero-vibrational levels of the S_1 $^1B_{3u}$ states of pyrene-h_{10} and pyrene-d_{10} are 1480 and 1470 ns, respectively, and the relaxation is considered to be dominated by the radiative process. For some vibrational levels, however, the lifetimes are remarkably shorter such as 765 ns at the 22^1 vibronic level of pyrene-h_{10} (ν_{22} (b_{1g}) ; C-H bending and skeletal deforming mode), indicating that nonradiative transition occurs at a specific vibrational level. In this study, we demonstrate that the main process is internal conversion to the S_0 ^1A_g state caused by nonadiabatic vibronic interaction via b_{3u} promoting modes.

Key words: , pyrene, fluorescence lifetime, internal conversion, ab initio theoretical calculation, molecular structure

[*]Corresponding author.
E-mail address: baba@kuchem.kyoto-u.ac.jp

1. Introduction

Radiationless transitions in large polyatomic molecules are of significant research interest and have been experimentally and theoretically investigated for various isolated molecules [1, 2, 3, 4]. For the S_1 $^1B_{2u}$ state of perylene, which is one of the typical polycyclic aromatic hydrocarbons (PAHs), we recently demonstrated that the main radiationless process is internal conversion (IC) to the S_0 state and is mode-selective [5, 6]. The fluorescence lifetime has been found to be considerably short for the specific vibrational level of skeletal deforming [7].

For pyrene, It has been demonstrated that the fluorescence lifetime is considerably long at the zero-vibrational level and becomes gradually shorter as the vibrational excess energy increased [8]. However, it is necessary to observe and analyze the fluorescence decay curve more carefully in order to obtain the accurate lifetime value, because the lifetime is long and the decay curve is easily distorted by the experimental setup. Although there has been no report of the accurate measurement of fluorescence quantum yield, radiationless transition processes are assumed to be all very slow and the relaxation in the S_1 state is dominated by the radiative transition. The rate of intersystem crossing (ISC) to the triplet state has been demonstrated to be negligible [9]. In the present work, we obtained the accurate fluorescence lifetime at each vibronic level in the S_1 state and examined the radiationless transitions.

The fluorescence excitation spectrum for the $S_1 \leftarrow S_0$ transition of pyrene has already been observed in a supersonic jet [8, 9, 10]. Although a normal-mode analysis in the S_1 state was carried out, the results were not reliable enough to assign the observed vibronic bands unambiguously. It is therefore necessary to reconsider the results on the basis of ab initio calculation at a sufficiently high level. The S_1 state has been identified to be $^1B_{3u}$ [9], in which the absorption band is weak and classified as ^1L_b [11]. The molecular structure, and the coordinate (rotational) axes of pyrene are illustrated in Fig. 1. The axis notation is important because the three coordinate axes are equivalent in D_{2h} symmetry. Here we take the x and y axes along the in-plane short and long axes, respectively. The z axis is perpendicular to the molecular plane. In this notation, ^1L_b is designated as $^1B_{3u}$, of which the absorption is weak and the radiative lifetime is long. In contrast, ^1L_a is designated as $^1B_{2u}$, of which the absorption is strong and the radiative lifetime is short. The strong transition moment is along the y axis. These expressions are identical

to those of linear polyacenes such as naphthalene and anthracene, and this axis notation is favorable to represent the electronic structure of PAHs in general. Mangle and Topp employed another axis notation, of which the expressions are obtained from ours by x, y, z, B_{1g}, B_{2g}, B_{3g}, B_{1u}, B_{2u}, B_{3u} $\rightarrow$ y, z, x, B_{3g}, B_{1g}, B_{2g}, B_{3u}, B_{1u}, B_{2u} [8].

The S_1 $^1B_{3u}$ state of naphthalene is also assigned to be ^1L_b. The fluorescence quantum yield is, however, remarkably small (~ 0.3) and the lifetime is approximately 300 ns [12]. Previously, we demonstrated that the lifetime was markedly shorter for some vibrational levels as a result of efficient IC to the S_0 state [13]. These results for pyrene and naphthalene are inconsistent with the general rule that the rate of radiationless transition is proportional to the density of coupling vibrational levels, and that the fluorescence quantum yield becomes smaller as the molecular size becomes larger [2, 4]. It is therefore unusual that no radiationless transition occurs efficiently in a large molecule such as pyrene. This is assumed to be strongly correlated with the fact that the geometrical structure at the zero-vibrational level and the potential energy curve in the S_1 state are very similar to those in the S_0 state. The vibrational energy may be changed appreciably at the specific normal mode, leading to the shorter fluorescence lifetime.

We performed accurate measurements of the vibrational energies and fluorescence lifetimes for the vibronic bands observed in the fluorescence excitation spectra of jet-cooled pyrene (pyrene-h_{10}) and perdeuterated pyrene (pyrene-d_{10}). We found that fluorescence lifetime was markedly short at some vibronic levels in the S_1 state, of which the vibrational modes were identified on the basis of the results of detailed ab initio calculations. In this article, we present the results of spectral analysis and theoretical calculations and discuss the vibrational structure and IC process at each vibrational level in the S_1 $^1B_{3u}$ state of pyrene.

2. Experimental

Pyrene-h_{10} (Wako Chemical, 99%) was recrystalized from ethanol and pyrene-d_{10} (Cambridge Isotope Laboratories, 98.4%) was used without further purification. The vapor was mixed with Ar gas (1.5 atm) in a stainless steel container of that was kept at 120 °C. The mixed gas was expanded into a high-vacuum chamber through a pulsed nozzle (an automobile electric fuel injector) to generate a supersonic jet, which was crossed with a pulsed laser beam at right angles. We used a tunable dye laser (Lambda Physik LPD

3002, $\Delta E = 0.1$ cm^{-1}, Exalite 398 and 416) pumped by an excimer laser (Coherent Compex Pro 110, 308 nm, 200 mJ). Fluorescence was collected using an ellipsoidal high-reflection mirror to a photomultiplier (Hamamatsu R928), which was set coaxially with the supersonic jet. The transient output was processed by a preamplifier (Stanford research R240, 50Ω, $\Delta t = 10$ ns) and was recorded as a fluorescence decay curve using a storage oscilloscope (LeCroy 9362) .

3. Results and Discussion

For the S$_1$ states of pyrene-h_{10} and pyrene-d_{10}, we observed the fluorescence excitation spectra in supersonic jets; the results are shown in Fig. 2. Almost all of the prominent vibronic bands are assigned to the transitions from the zero-vibrational level in the S$_0$ state to the a$_g$ and b$_{1g}$ vibrational levels in the S$_1$ state. The vibrational energies of the observed vibronic bands of pyrene-h_{10} and pyrene-d_{10} are listed in Tables 1 and 2, respectively.

Figure 3 depicts the fluorescence decay curves for the 0_0^0 and 22_0^1 (b$_{1g}$) ; $0_0^0 + 1111$ cm^{-1} bands of pyrene-h_{10}. The linewidth of the exciting laser light is 0.1 cm^{-1}, ensuring that a large number of rotational levels are coherently excited. All of the relaxation rates, however, are approximately identical and the fluorescence decay curve is expressed as a single-exponential function,

$$I_f(t) = a \, e^{-\frac{t}{\tau}} \; . \tag{1}$$

The observed curves were well fit by this function and the lifetime (τ) at the zero-vibrational levels of pyrene-h_{10} and pyrene-d_{10} were determined to be 1480 ns and 1470 ns, respectively. The observed values are slightly longer than those reported by Mangle and Topp [8]. This discrepancy is assumed to be due to the fluorescence detection system. The mean speed of molecules in a supersonic jet is over 500 m/s. The excited pyrene molecules translate nearly 1 mm during their lifetime, and some escape from the detection region. In our setup, the photomultiplier is set coaxially with the supersonic jet and the fluorescence is collected using an ellipsoidal reflection mirror, so that the time dependent loss of fluorescence intensity is negligible. It was found that the fluorescence lifetimes of pyrene-h_{10} were appreciably shorter for the specific b$_{1g}$ vibrational levels such as 22^1, 20^1, and 16^1.

For the high-vibrational levels, the decay curve consists of several components with different fluorescence lifetimes. This usually caused by mutual

interaction among the vibrational levels or accidental overlap of vibronic bands. In Fig. 4 are show the decay curves for the 6^1 (a_g) ; $0^0 + 1397$ cm^{-1} level of pyrene-h_{10}, and the 5^1 (a_g) ; $0^0 + 1447$ cm^{-1} level of pyrene-d_{10}. We approximately expressed the decay curve as a double-exponential function

$$I_f(t) = a_1 \, e^{-\frac{t}{\tau_1}} + a_2 \, e^{-\frac{t}{\tau_2}} \; . \tag{2}$$

The obtained lifetimes are tabulated in Tables 1 and 2. In order to understand these results, it is essential to analyze the electronic and vibrational structures of the pyrene molecule. We first performed ab initio calculations for the ground S_0 ^1A_g state to obtain the optimized geometrical structure and rotational constants using the Gaussian 09 program package [14]. The results are listed in Table 3(a) and are compared with the values that were experimentally obtained by ultrahigh-resolution laser spectroscopy [9]. We recently demonstrated that the MP2 method provided approximately the same values of rotational constants in the S_0 state as those obtained experimentally for benzene, naphthalene, and anthracene [15, 16]. For pyrene, however, we could not obtain such excellent results using the MP2, HF, and MP4 methods. The DFT(B3LYP)/cc-pVTZ calculation yielded the best result and the differences between the rotational constant values of the experimental and ab initio calculation are 0.08, 0.02, and 0.03% for A, B, and C, respectively. We calculated the vibrational energies for the a_g and b_{1g} normal modes in the S_0 state with the optimized structure by this calculational method. We performed least-squares fittings of the observed and calculated vibrational energies, and the best scaling factor was determined to be 0.983. The results are listed in Table 4; they show good agreement with the experimental values.

The transition energies of the $S_1 \leftarrow S_0$ and $S_2 \leftarrow S_0$ 0^0_0 bands of pyrene-h_{10} have been observed to be 27204 cm^{-1} and 30970 cm^{-1}, respectively [10, 9]. It has also been demonstrated by ultrahigh-resolution laser spectroscopy that the $S_1 \leftarrow S_0$ transition moment is in the direction of the in-plane short axis (x) and that the S_1 state is $^1B_{3u}$. Next, we performed ab initio calculations for the S_1 state. We tried several methods to obtain rotational constants with the optimized geometrical structure in the S_1 state. The results are presented in Table 3(b). The TD-DFT(cam-B3LYP)/6-31G(d,p) calculation provided values that were very close to the experimentally obtained rotational constants. The calculated excitation energies, however, do not show good agreement with the experimental values. In particular, the excitation

5

energy of the $^1B_{3u}$ state is delicate because the two excited-state configurations of HOMO → LUMO + 1 and HOMO − 1 → LUMO are nearly degenerate and are expressed by the same irreducible representation (Fig. 5). These are strongly mixed by the configuration interaction (CI). It is generally difficult to accurately evaluate the effect of CI on the excitation energies. As we could not find an excellent method, we employed the TD-DFT method, which provided very close values of rotational constants to the experimentally obtained ones, to calculate the oscillator strength (absorption intensity) and vibrational energies. The obtained oscillator strengths were $f_{S_1 \leftarrow S_0} = 0.0004$ and $f_{S_2 \leftarrow S_0} = 0.1617$. If the vibrational term is assumed to be unity, the radiative lifetime is given by [17]

$$\tau_r = 1.500 \, \frac{1}{\nu^2 f} \, . \tag{3}$$

We obtained $\tau_r(S_1) = 5100$ ns and $\tau_r(S_2) = 9.7$ ns. Here ν is the transition wavenumber in units of cm^{-1}. These values are consistent with the observed results that the $S_1 \leftarrow S_0$ absorption is weak and that the lifetime of the S_1 $^1B_{3u}$ state is fairly long. The calculated vibrational energies of the a_g and b_{1g} modes with the scaling factor of 0.975 are listed in Table 4. The scaling factors are appreciably different for the S_0 and S_1 states. It indicates that the calculated vibrational energies include some systematic errors arising from using different calculational methods and basis sets. The scaled vibrational energies, however, are in good agreement with expermentally obtained ones for both S_0 and S_1 states, and this normal mode analysis is considered to be reliable to unambiguously assign the observed vibronic bands.

In the fluorescence excitation spectra, the fundamental vibronic bands of the a_g and b_{1g} modes were observed with comparable intensity to the 0_0^0 band. The a_g modes are totally symmetric and the vibronic bands are observable for an allowed electronic transition. The transition moment is in the direction of the in-plane short axis (x) and the rotational transitions are of b-type. The b_{1g} modes are also observable in the fluorescence excitation spectrum, of which the intensities arise from nonadiabatic vibronic interaction with the S_2 $^1B_{2u}$ state. The transition moment is, therefore, in the direction of the in-plane long axis (y), and the rotational transitions are of a-type. In this case, the rotational envelope shows a sharp peak of the Q transitions at the band center. We identified a number of observed vibronic bands by these rotational contours. We also examined the calculated vibrational energies and the resultant assignments are listed in Tables 1 and 2.

6

The fluorescence lifetimes of vibrational levels are plotted against the vibrational excess energy in Fig. 6. The lifetime becomes gradually shorter as the vibrational excess energy increases and does not change significantly by deuterium substitution. The radiative lifetime is dependent on the electronic transition moment, but is independent of the atomic mass and vibrational energies in the Born−Oppenheimer approximation. The nonradiative lifetime is dominated by non-Born−Oppenheimer or nonadiabatic vibronic interaction, and generally becomes longer by deuterium substitution because the zero-point energy and vibrational overlap with coupling levels are smaller in the deuterated molecule [2, 3, 4]. Consequently, it is considered that the radiationless transition does not occur at the zero-vibrational level in the S_1 $^1B_{3u}$ state of pyrene and that is slightly enhanced at the high vibrational levels. The main process is expected to be IC to the S_0 ^1A_g state. The IC rate at the zero-vibrational level ($v' = 0$) of the S_1 state is given by [18]

$$
\begin{aligned}
W_{IC} \quad \propto \quad & \sum_i \left| \left\langle \phi_{S_0} \left| \frac{\partial}{\partial Q_i} \right| \phi_{S_1} \right\rangle \right|^2 \\
& \times \left| \left\langle \chi_{S_0}^{v''} \left| \frac{\partial}{\partial Q_i} \right| \chi_{S_1}^{v'=0} \right\rangle \right|^2 \\
& \times \delta(E_{S_1}^{v'=0} - E_{S_0}^{v''})
\end{aligned}
\tag{4}
$$

$$
\begin{aligned}
\approx \quad & \frac{\sum_i \left| \left\langle \phi_{S_0}(r, Q_0) \left| \left(\frac{\partial U(r,Q)}{\partial Q_i} \right)_{Q_0} \right| \phi_{S_1}(r, Q_0) \right\rangle \right|^2}{\{E_{S_1}(Q_0) - E_{S_0}(Q_0)\}^2} \\
& \times \left| \left\langle \chi_{S_0}^{v''}(Q_i) \left| \frac{\partial}{\partial Q_i} \right| \chi_{S_1}^{v'=0}(Q_i) \right\rangle \right|^2 \\
& \times \left| \prod_{j \neq i} \left\langle \chi_{S_0}^{v''}(Q_j) | \chi_{S_1}^{v'=0}(Q_j) \right\rangle \right|^2 \\
& \times \delta(E_{S_1}^{v'=0} - E_{S_0}^{v''}) \,.
\end{aligned}
\tag{5}
$$

The second factor is the nonadiabatic Franck-Condon overlap of a promoting mode and the third factor is the Franck-Condon overlap of other

modes. For the high vibrational levels in the S_0 state, this rate is zero if the potential energy curves along the normal coordinate of a promoting b_{3u} mode are identical for the S_0 and S_1 states. The equilibrium structures are considered to be nearly identical because the rotational constants are very similar for the S_0 and S_1 state [9]. The equilibrium C-C bond lengths calculated by the ab initio calculations with geometry optimization are not changed much upon the $S_1 \leftarrow S_0$ excitation, as shown in Table 5. The IC rate is, therefore, expected to be very small at the zero-vibrational level in the S_1 $^1B_{3u}$ state of pyrene.

It should be noted that the fluorescence lifetime is remarkably short for some specific vibrational levels. At the 22^1 level of pyrene-h_{10}, the lifetime is 765 ns, which is nearly half that at the zero-vibrational level. The ν_{22} mode is a vibration of C-H bending (mainly at C(2) and the equivalent positions) and skeletal deforming, so that the $22^1(b_{1g})$ level in the S_1 $^1B_{3u}$ state can be coupled with the b_{2u} high vibrational levels in the S_0 ^1A_g state (direct mechanism). The most probable candidate for the promoting mode is ν_{56} (b_{2u}), of which the nuclear displacement motions are very similar to those of ν_{22} (b_{1g}) with the opposite phase with respect to the long (y) axis. These normal coordinates are illustrated in Fig. 7. As for the 22^1 level, the potential curve in the S_1 state is considered to be identical to that in the S_0 state because the ν_{22} vibrational energies are just the same (1111 cm^{-1}) for the S_0 and S_1 states. We assume that the equilibrium structure is slightly different (distortion) [18] along this normal coordinate. The nonadiabatic Franck−Condon overlap is nonvanishing in this case and the IC occurs in the 22^1 (b_{1g}) vibronic level in the S_1 $^1B_{3u}$ state, leading to the shorter fluorescence lifetime. The absolute IC rate, is however, still longer than that of naphthalene or anthracene. It is possible to estimate the nonadiabatic Franck−Condon overlap value by numerical calculations of potentials and wavefunctions. However, the high level ab initio calculations are necessary to obtain reliable results for a large molecule such as pyrene. For the IC at the b_{1g} vibronic level, another mechanism is considerable, in which IC takes place by vibronic coupling with the S_2 $^1B_{2u}$ state and a b_{2u} promoting mode (indirect mechanism). The contribution is, however, considered to be small because the energy of the S_2 state is considerably higher than that of the 22^1 level in the S_1 state. In fact, the observed lifetimes at the b_{1g} levels are not different from those at the a_g levels.

Furthermore, the decay curve is expressed as a double-exponential function at several high vibrational levels. The fast lifetime is approximately 200

ns for all levels, which is attributed to vibronic coupling with the S_2 $^1B_{2u}$ state. In particular, the b_{1g} fundamental vibrational levels in the S_1 state are strongly coupled and the vibronic bands can be observed as sharp peaks in the fluorescence excitation spectrum. The other weakly coupled levels such as overtones and combination levels yield a broad spectral component. The congested rotational structure due to this vibronic coupling has been observed for the 3068 cm^{-1} level in the S_1 $^1B_{3u}$ state of naphthalene [13]. The intensity increases with the vibrational excess energy because the level density and coupling strength become larger. The S_2 zero-vibrational level is considered to be mixed with many vibrational levels of the S_1 state. The $S_2 \leftarrow S_0$ 0_0^0 band is broad and is accompanied by satellite bands [10]. This spectral feature is very similar to that of naphthalene [19]. The bandwidth is approximately 10 cm^{-1}, indicating that the $S_2 \rightarrow S_1$ IC occurs during 500 ps. In general, the S_2 state rapidly transitions to the S_1 state and is not fluorescent. This is in accordance with Kasha's rule that the emitting level of a given multiplicity is the lowest level of the multiplicity [20].

4. Summary

For the S_1 $^1B_{3u}$ state of pyrene-h_{10} and pyrene-d_{10}, we observed fluorescence excitation spectra and lifetimes for single vibronic level excitation. The vibrational energies and fluorescence lifetime have been accurately determined for the observed vibronic bands. The lifetimes at the zero-vibrational levels of pyrene-h_{10} and pyrene-d_{10} are 1480 ns and 1470 ns, respectively, and they become gradually shorter as the vibrational excess energy increases. This indicates that radiationless transitions are very slow in the S_1 $^1B_{3u}$ state of pyrene. For the $\nu_{22}(b_{1g})$ vibrational level of pyrene-h_{10}, however, the fluorescence lifetime is appreciably shorter (765 ns), as a result of IC to the S_0 ^1A_g state. The ν_{22} vibration is considered to be the promoting mode of IC in the S_1 state. The $\nu_{56}(b_{2u})$ vibration is presumed to be the promoting mode in the S_0 state, the nuclear motions of which are very similar to those of ν_{22} with the opposite phase. For high vibrational levels, the fluorescence decay curve is expressed by a double-exponential function. The fast decay component is originated from many vibrational levels in the S_1 state, which are mixed with the S_2 state by nonadiabatic vibronic interaction.

5. Acknowledgements

References

[1] P. Avouris, W. M. Gelbart, M. A. El-Sayed, Chem. Rev. 77 (1977) 793.

[2] M. Bixon, J. Jortner, J. Chem. Phys. 48 (1968) 715.

[3] K. F. Freed, Acc. Chem. Res. 1 (1978) 74.

[4] S. H. Lin, J. Chem. Phys. 44 (1966) 3759.

[5] Y. Kowaka, Y. Suganuma, N. Ashizawa, N. Nakayama, H. Goto, T. Ishimoto, U. Nagashima, M. Baba, J. Mol. Spectrosc. 260 (2010) 72.

[6] Y. Suganuma, Y. Kowaka, N. Ashizawa, N. Nakayama, T. Ishimoto, U. Nagashima, T. Yamanaka, T. Ueda, N. Nishi, M. Baba, Mol. Phys. 109 (2011) 1831.

[7] A. J. Kaziska, S. A. Wittmeyer, A. L. Motyka, M. R. Topp, Chem. Phys. Lett. 154 (1989) 199.

[8] E. A. Mangle, M. R. Topp, J. Phys. Chem. 90 (1986) 802.

[9] M. Baba, M. Saitoh, Y. Kowaka, K. Taguma, K. Yoshida, Y. Semba, S. Kasahara, Y. Ohshima, T. Yamanaka, Y.-C. Hsu, S. H. Lin, J. Chem. Phys. 131 (2009) 224318.

[10] N. Ohta, H. Baba, G. Marconi, Chem. Phys. Lett. 133 (1987) 222.

[11] J. R. Platt, J. Chem. Phys. 17 (1949) 484.

[12] F. M. Behlen, S. A. Rice, J. Chem. Phys. 75 (1981) 5672.

[13] K. Yoshida, Y. Semba, S. Kasahara, T. Yamanaka, M. Baba, J. Chem. Phys. 130 (2009) 194304.

[14] M. J. Frisch, G. W. Trucks, H. B. Schlegel, G. E. Scuseria, M. A. Robb, J. R. Cheeseman, G. Scalmani, V. Barone, B. Mennucci, A. F. Izmaylov, J. Bloino, G. Zheng, J. L. Sonnenberg, M. Hada, M. Ehara, K. Toyota, R. Fukuda, J. Hasegawa, M. Ishida, T. Nakajima, Y. Honda, O. Kitao, H. Nakai, T. Vreven, J. A. Montgomery, Jr., J. E. Peralta, F. Ogliaro, M. Bearpark, J. J. Heyd, E. Brothers, K. N. Kudin, V. N. Staroverov, R. Kobayashi, J. Normand, K. Raghavachari, A. Rendell, J. C. Burant,

S. S. Iyengar, J. Tomasi, M. Cossi, N. Rega, J. M. Millam, M. Klene, J. E. Knox, J. B. Cross, V. Bakken, C. Adamo, J. Jaramillo, R. Gomperts, R. E. Stratmann, O. Yazyev, A. J. Austin, R. Cammi, C. Pomelli, J. W. Ochterski, R. L. Martin, K. Morokuma, V. G. Zakrzewski, G. A. Voth, P. Salvador, J. J. Dannenberg, S. Dapprich, A. D. Daniels, O. Farkas, J. B. Foresman, J. V. Ortiz, J. Cioslowski, D. J. Fox, Gaussian09, Revision A.02, Gaussian Inc., Wallingford, CT, 2009.

[15] M. Baba, Y. Kowaka, U. Nagashima, T. Ishimoto, H. Goto, N. Nakayama, J. Chem. Phys. 135 (2011) 054305.

[16] M. Baba, M. Saitoh, K. Taguma, K. Shinohara, K. Yoshida, Y. Semba, S. Kasahara, N. Nakayama, H. Goto, T. Ishimoto, U. Nagashima, J. Chem. Phys. 101 (2009) 134315.

[17] R. A. Becker, Theory and Interpretation of Fluorescence and Phosphorescence, John Wiley & Sons, New York, 1969.

[18] W. Siebrand, J. Chem. Phys. 46 (1967) 440.

[19] S. M. Beck, D. E. Powers, J. B. Hopkins, R. E. Smalley, J. Chem. Phys. 73 (1980) 2019.

[20] M. Kasha, Disc. Faraday Soc. 9 (1950) 14.

Table 1. Vibrational energies (cm^{-1}), lifetimes (ns) and assignments of the bands observed in the fluorescence excitation spectrum of the S_1 $^1\mathrm{B}_{3u} \leftarrow \mathrm{S}_0$ $^1\mathrm{A}_g$ transition of pyrene-h_{10}.

Vibrational energy	Lifetimes			Assignment
	τ_1	τ_2	(a_2) [a]	
0		1480		0_0^0 (27204 cm^{-1})
393		1190		13_0^1 (a_g)
443		1190		
449		1250		25_0^1 (b_{1g})
453		1250		
494		1210		24_0^1 (b_{1g})
551		1190		
572		1080		12_0^1 (a_g)
673		957		
709		973		
724		1060		
730		1200		23_0^1 (b_{1g})
782		1170		11_0^1 (a_g)
1023	238	905	(1.9)	10_0^1 (a_g)
1111		765		22_0^1 (b_{1g})
1144		1120		9_0^1 (a_g)
1250	147	837	(3.4)	20_0^1 (b_{1g})
1282	160	853	(1.9)	
1298	220	867	(0.84)	
1357	75	974	(10.1)	19_0^1 (b_{1g})
1397	147	1090	(1.3)	6_0^1 (a_g)
1575	250	794	(2.2)	16_0^1 (b_{1g})
1681		840		4_0^1 (a_g)
1699		840		
1841		783		
1902	204	804	(3.7)	
1942	178	664	(3.2)	

[a]Relative values assuming $a_1 = 1$.

Table 2. Vibrational energies (cm^{-1}), lifetimes (ns) and assignments of the bands observed in the fluorescence excitation spectrum of the S$_1$ ^{1}B$_{3u}$ ← S$_0$ ^{1}A$_g$ transition of pyrene-d_{10}.

Vibrational energy	Lifetimes			Assignment
	τ_1	τ_2	(a_2) [a]	
0		1470		0_0^0 (27283 cm^{-1})
384		1270		13_0^1 (a$_g$)
431		1300		25_0^1 (b$_{1g}$)
460		1220		24_0^1 (b$_{1g}$)
544		1240		12_0^1 (a$_g$)
607		1280		
645		1140		
682		1180		23_0^1 (b$_{1g}$)
698		1220		
735		1180		11_0^1 (a$_g$)
743		1230		
770	205	1170	(4.5)	
832	188	1130	(4.5)	10_0^1 (a$_g$)
856		1200		9_0^1 (a$_g$)
927		1170		
932		1160		21_0^1 (b$_{1g}$)
1008		1090		
1225		972		19_0^1 (b$_{1g}$)
1231		989		7_0^1 (a$_g$)
1245		951		
1289		1050		
1323		1080		
1348		970		
1382	201	1060	(2.1)	
1390		929		17_0^1 (b$_{1g}$)
1403		978		18_0^1 (b$_{1g}$)
1430		905		6_0^1 (a$_g$)
1447	214	871	(9.2)	5_0^1 (a$_g$)
1557		882		16_0^1 (b$_{1g}$)
1822		777		

[a]Relative values assuming $a_1 = 1$.

Table 3. Experimental and calculated rotational constants (cm^{-1}) in the S_0 ^1A_g state of pyrene-h_{10}.

| | Rotational constants | | |
	A	B	C
(a) S_0 ^1A_g			
exp [a]	0.0339147	0.0186550	0.0120406
DFT(B3LYP)/cc-pVTZ	0.0339412	0.0186518	0.0120370
MP2/cc-pVTZ	0.0338789	0.0186461	0.0120269
HF/6-31G(d,p)	0.0340442	0.0187661	0.0120976
MP4(SDQ)/6-31G(d,p)	0.0336811	0.0185206	0.0119497
(b) S_1 $^1B_{3u}$			
exp [a]	0.0336223	0.0184864	0.0119329
TD-DFT(cam-B3LYP)/6-31G(d,p)	0.0336785	0.0185127	0.0119752
SAC-CI/6-31G(d,p)	0.0335954	0.0185335	0.0119442
CASSCF/6-31G(d,p)	0.0338710	0.0184180	0.0119305
RCIS/6-31G(d,p)	0.0341973	0.0184529	0.0119855

[a] Ref.9.

Table 4. Calculated and observed a_g and b_{1g} vibrational energies (cm^{-1}) in the S_0 ^1A_g and S_1 $^1B_{3u}$ states of pyrene-h_{10} and pyrene-d_{10}.

			Pyrene-h_{10}		Pyrene-d_{10}	
			S_0 ^1A_g	S_1 $^1B_{3u}$	S_0 ^1A_g	S_1 $^1B_{3u}$
	Number	Vibration type	Calc.[a] (Obs.) [b]	Calc.[c] (Obs.)[d]	Calc.[a]	Calc.[c] (Obs.)[d]
a_g	1	C-H stretch	3143	3105	2357	2299
	2	C-H stretch	3134	3089	2347	2288
	3	C-H stretch	3118	3077	2326	2268
	4	C-C stretch	1646 (1624)	1663 (1681)	1689	1646
	5	C-C stretch + C-H bend	1572	1530	1509	1472 (1447)
	6	C-C stretch	1406 (1410)	1442 (1397)	1465	1429 (1430)
	7	ring deform	1333 (1326)	1326	1305	1273 (1231)
	8	ring deform + C-H bend	1245 (1238)	1257 (1250)	1181	1152
	9	C-H bend	1152 (1140)	1141 (1144)	853	860 (856)
	10	ring deform + C-H bend	1076 (1072)	1046 (1023)	882	832 (832)
	11	ring deform	804 (805)	779 (782)	753	734 (735)
	12	ring breathing	587 (593)	570 (572)	559	545 (549)
	13	ring deform	406 (402)	393 (393)	395	385 (384)
b_{1g}	14	C-H stretch	3126	3082	2334	2276
	15	C-H stretch	3115	3071	2322	2264
	16	C-C stretch	1608 (1571)	1563 (1575)	1584	1545 (1557)
	17	C-C stretch + C-H bend	1513 (1513)	1492	1460	1424 (1403)
	18	C-C stretch	1415	1425	1448	1412 (1390)
	19	C-H bend + ring deform	1381 (1372)	1408 (1357)	1259	1228 (1225)
	20	C-H bend + ring deform	1247 (1238)	1242 (1250)	1064	1038
	21	C-H bend	1183 (1212)	1167	959	935 (932)
	22	C-H bend + ring deform	1112 (1111)	1101 (1111)	855	834
	23	ring deform	739 (735)	729 (730)	701	683 (683)
	24	ring deform	501 (500)	499 (494)	472	461 (459)
	25	ring deform	456 (451)	449 (449)	443	432 (432)

[a] Results of DFT(B3LYP)/cc-pVTZ are scaled by 0.983.
[b] Determined using the dispersed fluorescence spectrum [Ref.9].
[c] Results of TD-DFT(cam-B3LYP)/6-31G(d,p) are scaled by 0.975.
[d] Determined using the fluorescence excitation spectrum in the present work.

Table 5. Calculated C-C bond lengths (Å) of pyrene in the S_0 ^1A_g and S_1 $^1B_{3u}$ states.

	S_0 $^1A_g{}^a$	S_1 $^1B_{3u}{}^b$
$R_{\text{C-C}}(\ 1\text{-}\ 2)$	1.3882	1.4002
$R_{\text{C-C}}(\ 2\text{-}11)$	1.3988	1.4020
$R_{\text{C-C}}(11\text{-}\ 3)$	1.4331	1.4216
$R_{\text{C-C}}(\ 3\text{-}\ 4)$	1.3552	1.3715
$R_{\text{C-C}}(11\text{-}15)$	1.4230	1.4487
$R_{\text{C-C}}(15\text{-}16)$	1.4217	1.4217

[a] DFT(B3LYP)/cc-pVTZ calculation.
[b] TD-DFT(cam-B3LYP)/6-31G(d,p) calculation.

Figure Captions

Fig. 1 Molecular structure and coordinate (rotational) axes of pyrene.

Fig. 2 Fluorescence excitation spectra of jet-cooled (a) pyrene-h_{10} and (b) pyrene-d_{10}.

Fig. 3 Fluorescence decay curves for excitations of (a) 0_0^0 and (b) 22_0^1 (0_0^0 + 1111 cm^{-1}) bands of pyrene-h_{10}.

Fig. 4 Fluorescence decay curves for excitations of (a) 6_0^1 band of pyrene-h_{10} and (b) 5_0^1 band of pyrene-d_{10}.

Fig. 5 π molecular orbitals and the electronic configurations for the S$_1$ ^{1}B$_{3u}$ and S$_2$ ^{1}B$_{2u}$ states.

Fig. 6 Fluorescence lifetimes for vibronic levels in the S$_1$ ^{1}B$_{3u}$ states of (a) pyrene-h_{10} and (b) pyrene-d_{10}. Circles, squares, and triangles indicate the a$_g$, b$_{1g}$, and unassigned levels, respectively.

Fig. 7 Normal coordinates of (a) ν_{22} (b$_{1g}$) and (b) ν_{56} (b$_{2u}$). The observed ν_{22} and calculated ν_{56} vibrational energies are shown below.
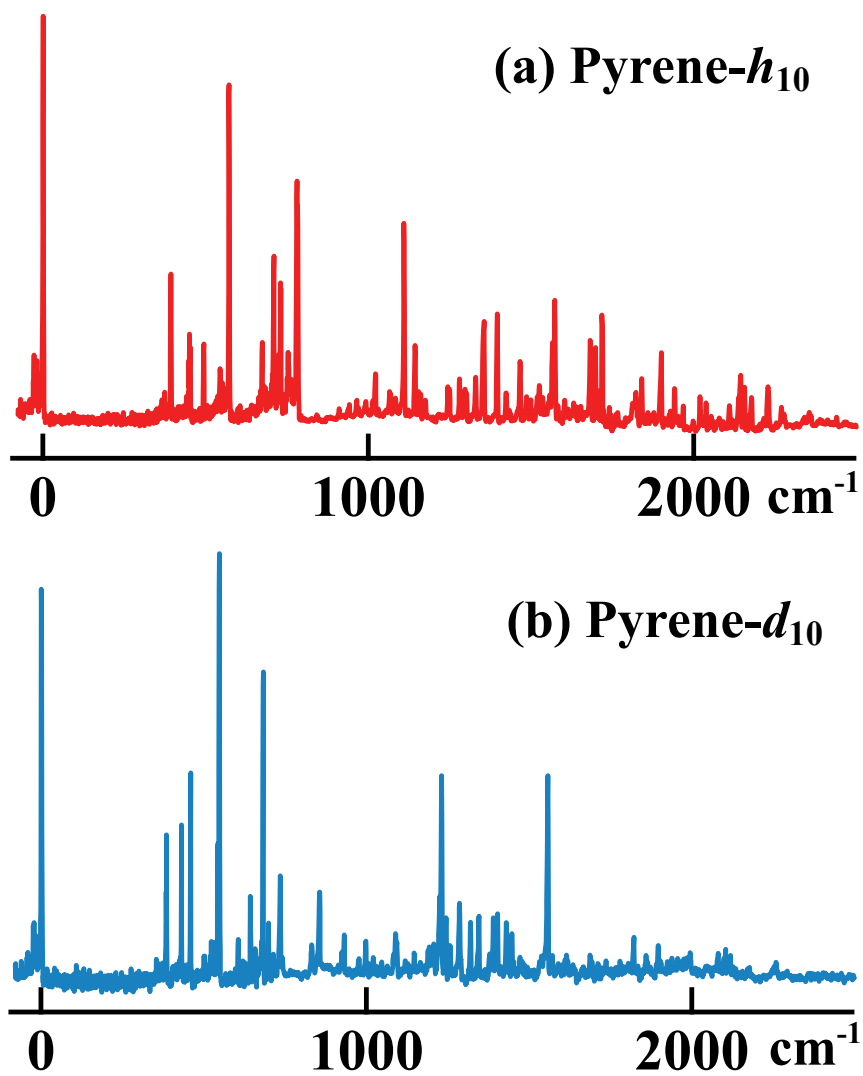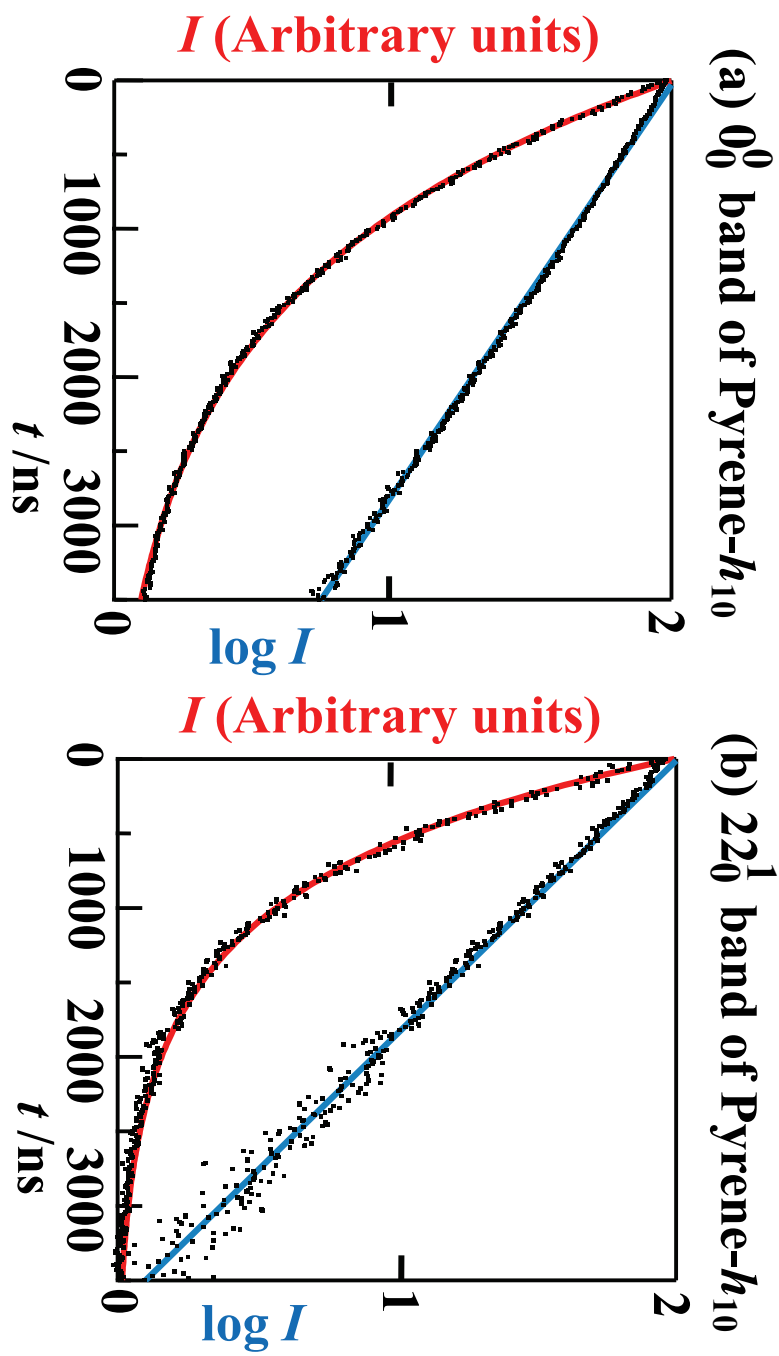
Fig. 1. Y. Kowaka *et al.*

(a) Pyrene-*h*₁₀

(b) Pyrene-*d*₁₀

Fig. 2.   Y. Kowaka *et al.*

(a) 0_0^0 band of Pyrene-h_{10}

(b) 22_0^1 band of Pyrene-h_{10}

I (Arbitrary units)

log *I*

t /ns
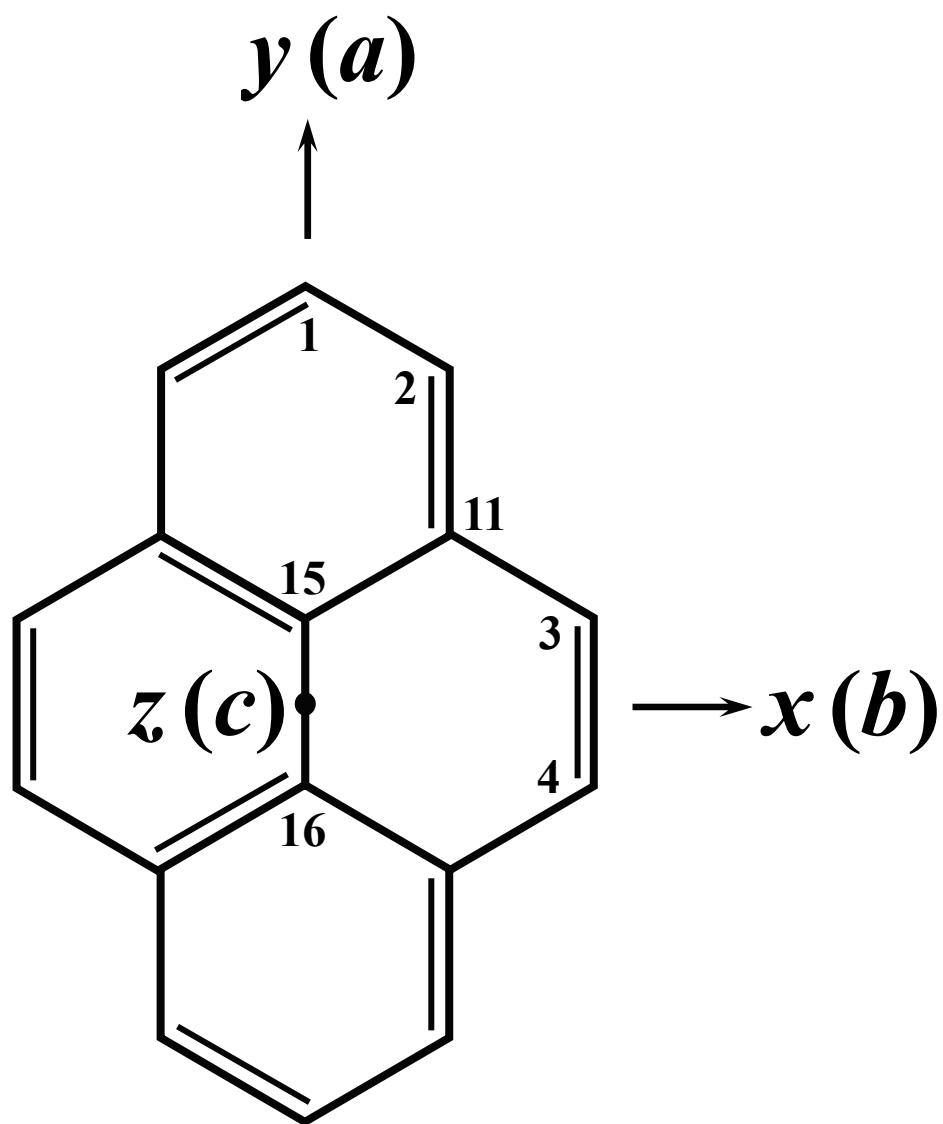
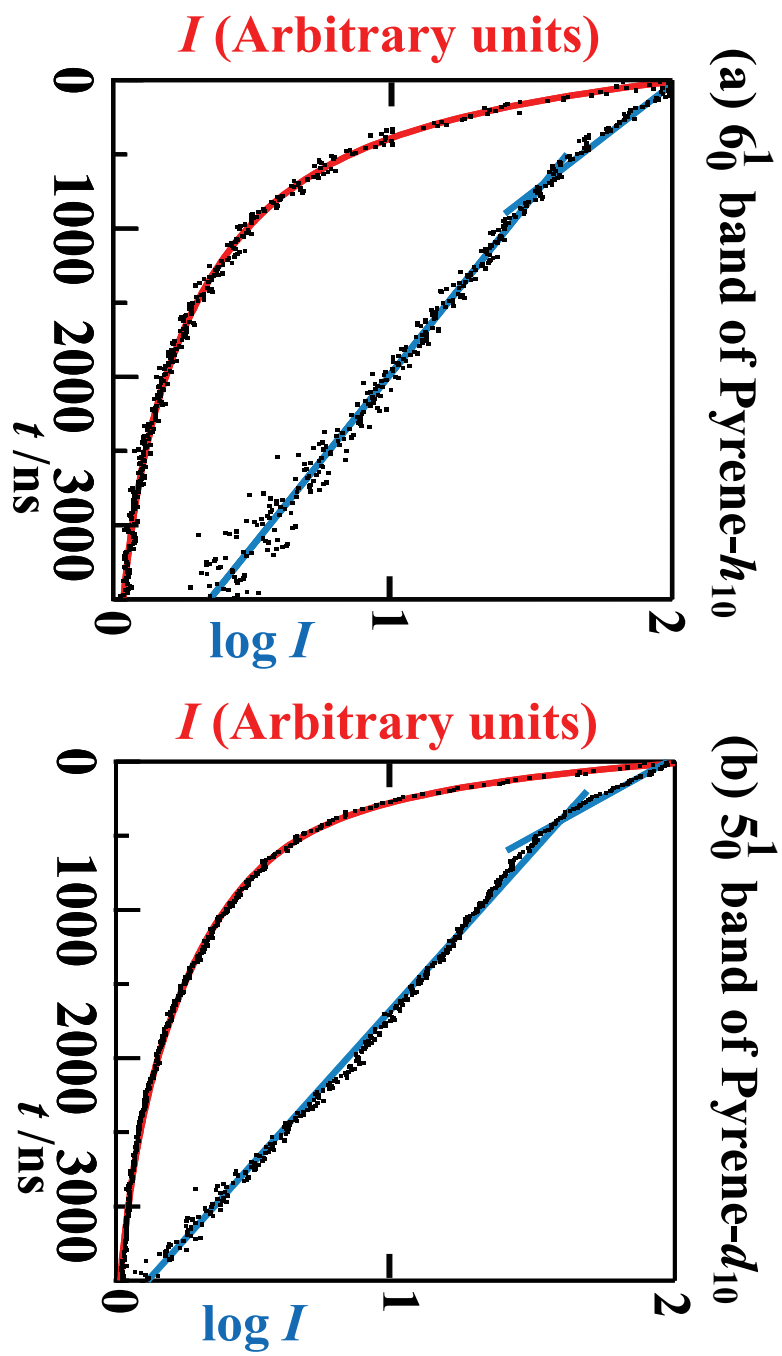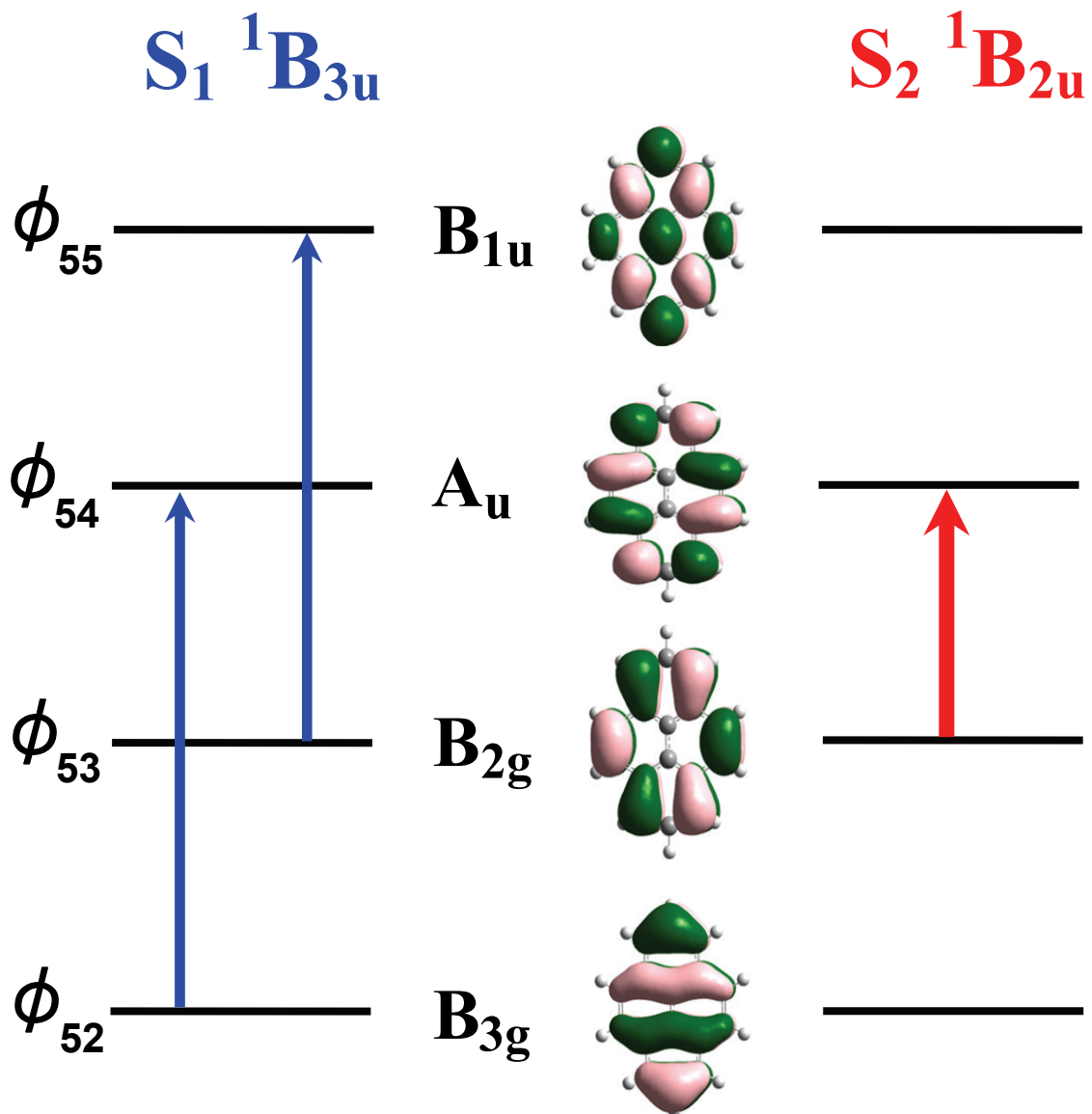**Fig. 3.   Y. Kowaka *et al.***

Fig. 4.   Y. Kowaka *et al.*
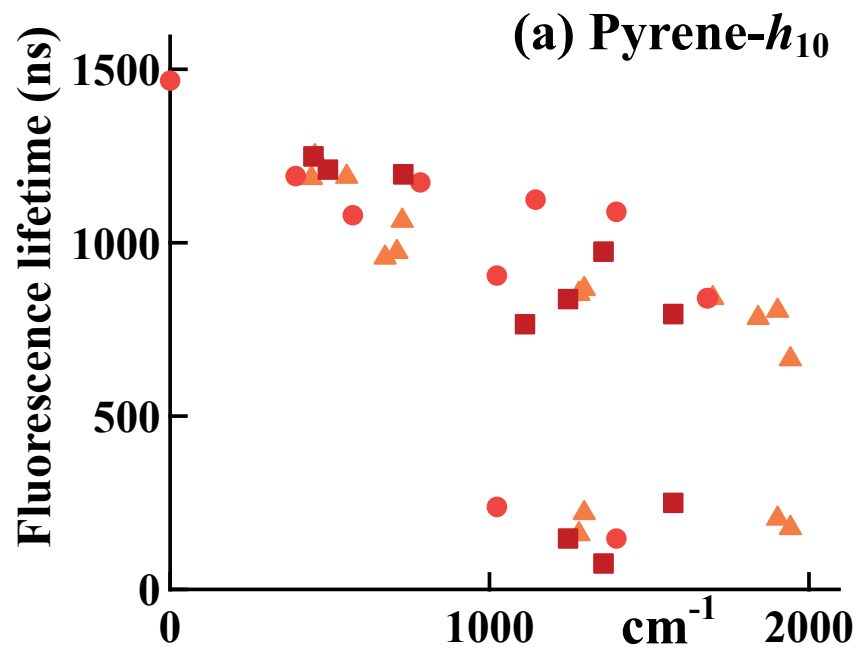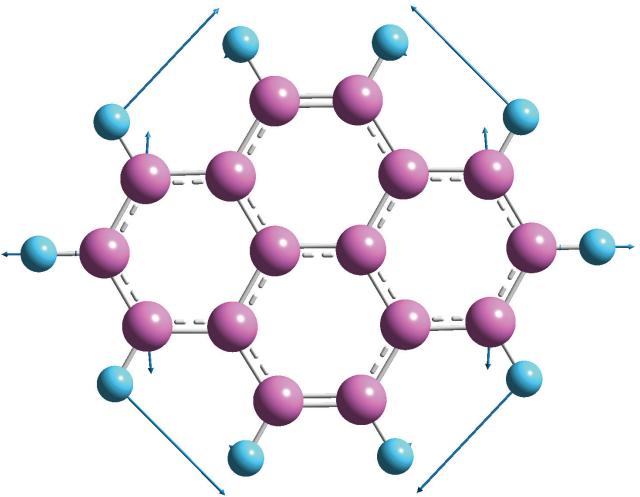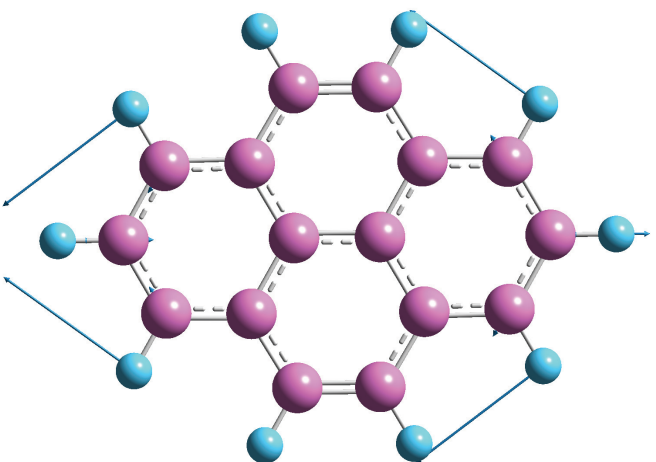
S_1 $^1B_{3u}$

ϕ_{55} B_{1u}

ϕ_{54} A_u

ϕ_{53} B_{2g}

ϕ_{52} B_{3g}

S_2 $^1B_{2u}$

Fig. 5.   Y. Kowaka *et al.*

(a) Pyrene-h_{10}

(b) Pyrene-d_{10}
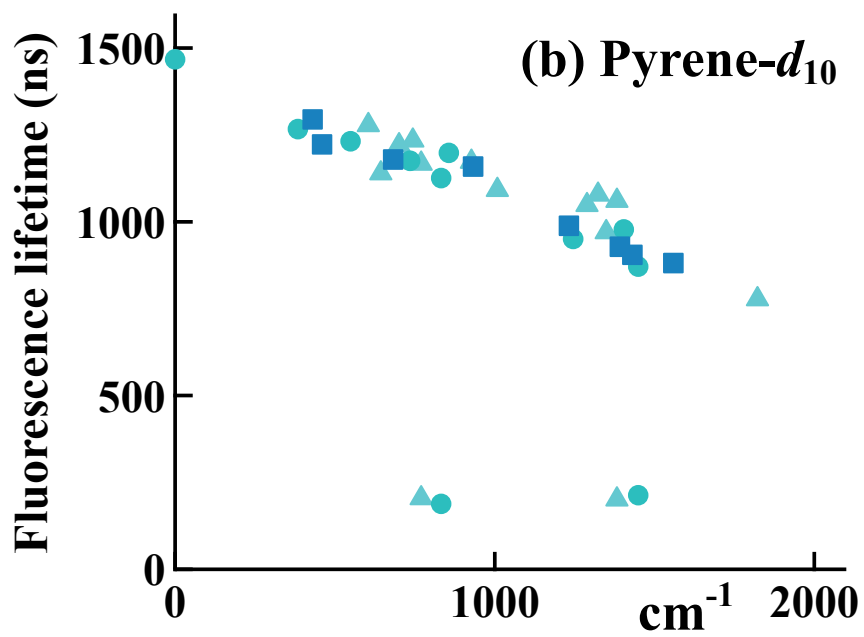
Fig. 6.   Y. Kowaka *et al.*

(a) ν_{22} (b$_{1g}$)

S$_1$	1111 cm^{-1}	
S$_0$	1111 cm^{-1}	

(b) ν_{56} (b$_{2u}$)

S$_1$	1066 cm^{-1}	
S$_0$	1092 cm^{-1}	

Fig. 7.   Y. Kowaka *et al.*